Improved tetrahedron method for the Brillouin-zone integration applicable to response functions

Mitsuaki Kawamura,[1,*] Yoshihiro Gohda,[1] and Shinji Tsuneyuki[1,2]

[1]*Department of Physics, University of Tokyo, Tokyo 113-0033, Japan*
[2]*Institute for Solid State Physics, University of Tokyo, Kashiwa 277-8581, Japan*

We improve the linear tetrahedron method to overcome systematic errors due to overestimations (underestimations) in integrals for convex (concave) functions, respectively. Our method is applicable to various types of calculations such as the total energy, the charge (spin) density, response functions, and the phonon frequency, in contrast with the Blöchl correction, which is applicable to only the first two. We demonstrate the ability of our method by calculating phonons in MgB_2 and fcc lithium.

I. INTRODUCTION

In calculations of periodic systems on the basis of density functional theory (DFT) [1], integrals of matrix elements over the Brillouin zone (BZ) are evaluated to obtain various physical quantities of solids including the total energy, the electron (spin) density, the density of states, response functions, and the phonon frequency. Since this integral with respect to the Bloch wave vector $\boldsymbol{k}$ is replaced with a summation over a range of points described by a discrete variable $\boldsymbol{k}$, approximation schemes employed for this summation can significantly affect the accuracy and computational costs. Accurate integration using a modest number of $\boldsymbol{k}$ points is even more important for hybrid-DFT [2] and GW approximations [3], because in these cases the computational cost is proportional to the square of the number of $\boldsymbol{k}$ points, whereas standard semilocal approximations have a linear dependence.

There are two kinds of schemes to perform such an integration over the $\boldsymbol{k}$ points, namely, the broadening method [4] and the tetrahedron method [5]. In the broadening method, we replace the delta function with a smeared function which has a finite broadening width; we have to check the convergences about both the broadening width and the number of $\boldsymbol{k}$ points to obtain accurate results. In the tetrahedron method, we perform analytical integration in tetrahedral regions covering the BZ with the piecewise linear interpolation of a matrix element. Unlike the broadening method, we have to check the convergence only about the number of $\boldsymbol{k}$ points. The tetrahedron method is applied to calculations of susceptibility [6], phonon frequency [7], phonon line width [8], and the local Green's function as part of the dynamical mean field theory in the Hubbard model [9].

However, the tetrahedron method has a drawback: if a matrix element $A_{\boldsymbol{k}}$ is a convex (concave) function of $\boldsymbol{k}$, this method systematically overestimates (underestimates) its contribution to the integral due to the linear interpolation involved. Although this can be avoided by using the quadratic interpolation, we cannot perform analytical integration straightforwardly in such a case. The Blöchl correction [10] was invented to overcome this issue by utilizing the following two facts: (i) the difference between the linear interpolation integration and that using the quadratic interpolation is approximately proportional to the

second derivative of $A_{\boldsymbol{k}}$ integrated over the occupied region; (ii) although $\partial^2 A_{\boldsymbol{k}}/\partial k^2$ cannot be evaluated within the framework of linear interpolation, we can perform the volume integral by replacing it with the Fermi surface integration of the first derivative of $A_{\boldsymbol{k}}$ (which can be evaluated by linear interpolation) using the Gauß theorem. Using this method we can reduce the number of $\boldsymbol{k}$ points to obtain converged results for total energies and charge densities. However, in the calculation of response functions or phonon frequencies, the integral $\int_{\epsilon_{\boldsymbol{k}} < \epsilon_F} d^3 k A_{\boldsymbol{k}}/(\epsilon_F - \epsilon_{\boldsymbol{k}})$ appears, where $A_{\boldsymbol{k}}$ is an arbitrary function of $\boldsymbol{k}$. In this case, the Blöchl correction is inapplicable because we cannot perform the Fermi surface integration when $\partial(A_{\boldsymbol{k}}/(\epsilon_F - \epsilon_{\boldsymbol{k}}))/\partial k$ is singular.

In this work, we develop a newly improved tetrahedron method that is applicable to calculations involving integrations of functions with singularities on the Fermi surfaces. It is constructed by means of a higher order interpolation and the least-squares method. We apply our method to the BZ integration in calculations of phonon frequencies based on density functional perturbation theory (DFPT) [11]. Following that we successfully calculate the frequency of phonons in MgB_2 and fcc Li. In contrast, it is difficult to achieve convergence in this calculation using conventional methods because the phonons in these materials couple strongly with electrons in the vicinity of Fermi surfaces [12,13]. In Sec. II, we describe our new tetrahedron method in detail after summarizing the conventional linear tetrahedron method and the Blöchl correction. Section III shows how our method improves the convergence about the number of $\boldsymbol{k}$ points in the calculation of phonons, followed by the conclusion in Sec. IV.

II. METHOD

In this section, we introduce our new tetrahedron method; we begin with the standard linear tetrahedron method and the Blöchl correction to explain why these methods are not necessarily efficient in calculating response functions such as phonon frequencies.

A. The linear tetrahedron method and its drawbacks

We overview the general procedure of the tetrahedron method and its drawbacks. We calculate the integral

$$\int d^3 k A_{\boldsymbol{k}} B(\epsilon_{\boldsymbol{k}}), \qquad (1)$$
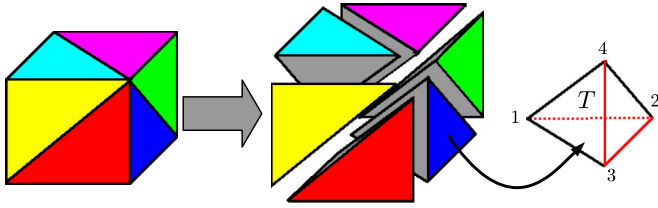
*kawamura@cms.phys.s.u-tokyo.ac.jp

FIG. 1. (Color online) Subcell division into six tetrahedra and numbering of the tetrahedron corners; the red lines in the rightmost tetrahedron are the edges of the subcell.
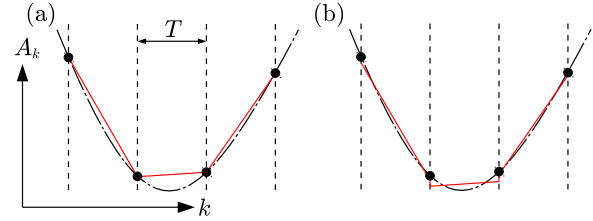

FIG. 2. (Color online) Two kinds of approximations of the matrix element. True and approximated matrix elements A_T are depicted as black dash-doted lines and red solid lines, respectively; the black points indicate the matrix elements A_k for a given value of k; the dashed lines indicate the boundaries of the tetrahedra. (a) The liner interpolated function A_T^1 is always smaller (larger) than the true function A_T in the case of a convex (concave) function. (b) The leveled linear function is a better approximation of the true function.

on the basis of the linear tetrahedron method, where $B(\epsilon_k)$ is a function of the orbital energy such as $\theta(\epsilon_F - \epsilon_k)$, $\delta(\epsilon_F - \epsilon_k)$, or $\theta(\epsilon_F - \epsilon_k)/(\epsilon_F - \epsilon_k)$. Here, $\theta(x)$ is the Heaviside step function. First, we divide a subcell into six tetrahedra (Fig. 1); this subcell is partitioned with the uniform k-point mesh; for convenience, we number the corners of each tetrahedron from 1 to 4 along specific edges of the subcell (see Fig. 1). The contribution of this tetrahedron (T) to the integral (1) is

$$6V_T \int_0^1 dx \int_0^{1-x} dy \int_0^{1-x-y} dz A_T(s) B[\epsilon_T(s)], \quad (2)$$

where $s = (x,y,z)$, and

$$A_T(s) \equiv A_{k_1^T(1-x-y-z)+k_2^T x+k_3^T y+k_4^T z}, \quad (3)$$

$$\epsilon_T(s) \equiv \epsilon_{k_1^T(1-x-y-z)+k_2^T x+k_3^T y+k_4^T z}, \quad (4)$$

where k_i^T is the k point of the ith corner of T. In the linear tetrahedron method, we approximate A_T and ϵ_T with linear functions:

$$A_T^1(s) = A_1(1-x-y-z) + A_2 x + A_3 y + A_4 z, \quad (5)$$

$$\epsilon_T^1(s) = \epsilon_1(1-x-y-z) + \epsilon_2 x + \epsilon_3 y + \epsilon_4 z, \quad (6)$$

where A_i and ϵ_i are the matrix element and the orbital energy at the ith corner, respectively. The integration (2) with formulas (5) and (6) is performed *analytically*.

However, linear interpolation has a drawback: if the matrix element $A_T(s)$ is a convex function within the tetrahedron T, the interpolated function $A_T^1(s)$ becomes $A_T^1(s) \geqslant A_T(s)$ in T; hence, the integral is systematically overestimated. If $A_T(s)$ is a concave function, the sign of the inequality is reversed [see Fig. 2(a)].

B. The Blöchl correction and its limitation

In the special case that the integral (1) becomes

$$\int d^3 k A_k \theta(\epsilon_F - \epsilon_k), \quad (7)$$

we can overcome the drawback of the linear tetrahedron method by considering the curvature of A_k within the framework of the linear interpolation [10]; this type of integration appears in the calculations of total energies or charge (spin) densities. In this case, we can evaluate the difference between the integral (7) with the linear interpolation of A_k (A^{lin}) and that with the quadratic interpolation (A^{quad}) as follows. First,

we write this difference as

$$\Delta A \equiv A^{\text{quad}} - A^{\text{lin}} = \sum_T^{\epsilon_k \leqslant \epsilon_F} \sum_{ij} C_{ij}^T \left\langle \frac{\partial^2 A_k}{\partial k_i \partial k_j} \right\rangle_T, \quad (8)$$

where C_{ij}^T is the form factor describing the shape and the orientation of the tetrahedron as follows,

$$C_{ij}^T = \frac{1}{40} \left[\sum_{l=1}^4 (k_l^T)_i \sum_{m=1}^4 (k_m^T)_j - 4 \sum_{l=1}^4 (k_l^T)_i (k_l^T)_j \right], \quad (9)$$

and $\langle \cdots \rangle_T$ indicates an integration in the tetrahedron T. Now, we replace $\partial^2 A_k / \partial k^2$ with $\partial A_k / \partial k$ because the former cannot be evaluated in the framework of the linear interpolation, but the latter can be. We assume that the form factor is a constant over the entire BZ ($C_{ij}^T \approx C_{ij}$), and then we apply the Gauß theorem:

$$\Delta A \approx \sum_{ij} C_{ij} \int_{\epsilon_k < \epsilon_F} d^3 k \frac{\partial^2 A_k}{\partial k_i \partial k_j}$$

$$= \sum_{ij} C_{ij} \int_{\epsilon_k = \epsilon_F} d^2 k \frac{(\nabla_k \epsilon_k)_i}{|\nabla_k \epsilon_k|} \frac{\partial A_k}{\partial k_j}$$

$$\approx \sum_T^{\text{Fermi surface}} \sum_{ij} C_{ij}^T \left\langle \frac{(\nabla_k \epsilon_k)_i}{|\nabla_k \epsilon_k|} \frac{\partial A_k}{\partial k_j} \right\rangle_T. \quad (10)$$

However, when we calculate an integral such as

$$\int d^3 k A_k \frac{\theta(\epsilon_F - \epsilon_k)}{\epsilon_F - \epsilon_k} \quad (11)$$

(this kind of integration appears in the calculations of response functions and phonon frequencies), the difference associated with the two kinds of interpolation becomes

$$\Delta A = \sum_T^{\epsilon_k < \epsilon_F} \sum_{ij} C_{ij}^T \left\langle \frac{\partial^2 A_k}{\partial k_i \partial k_j} \right\rangle_T G(\epsilon_k, \nabla_k \epsilon_k), \quad (12)$$

where $G(\epsilon_k, \nabla_k \epsilon_k)$ is a complicated function of ϵ_k and $\nabla_k \epsilon_k$; therefore, we cannot apply the Blöchl correction because we cannot replace $\partial^2 A_k / \partial k^2$ with $\partial A_k / \partial k$ as before. This is due to the presence of the energy denominator; hence, we have to start with another concept to overcome this issue.

TABLE I. Points for constructing a third-order interpolation function.

Nearest-neighbor points on extended lines of each edge of T (green balls in Fig. 3).		
$k_5 = 2k_1 - k_2$	$k_9 = 2k_1 - k_3$	$k_{13} = 2k_1 - k_4$
$k_6 = 2k_2 - k_3$	$k_{10} = 2k_2 - k_4$	$k_{14} = 2k_2 - k_1$
$k_7 = 2k_3 - k_4$	$k_{11} = 2k_3 - k_1$	$k_{15} = 2k_3 - k_2$
$k_8 = 2k_4 - k_1$	$k_{12} = 2k_4 - k_2$	$k_{16} = 2k_4 - k_3$
Remaining corners of tetrahedra that share surfaces with T (blue balls in Fig. 3).		
$k_{17} = k_4 - k_1 + k_2$	$k_{18} = k_1 - k_2 + k_3$	
$k_{19} = k_2 - k_3 + k_4$	$k_{20} = k_3 - k_4 + k_1$	

C. A newly improved tetrahedron method applicable to response functions

The systematic error of the tetrahedron method is a result of the *linear interpolation*. Although we can avoid this problem if we use higher order interpolation, the integral (2) becomes unsolvable analytically. The real question is, how can we improve the *linear* approximation of the matrix elements? The answer is to employ *leveling* rather than interpolating [see Fig. 2(b)]. The procedure is explained below.

(1) We construct the Nth polynomial $A_T^N(s)$ from A_k and k using the corners of a tetrahedron T and some additional surrounding points for sampling.

(2) We fit a linear function

$$A_T^{LSM}(s) = \bar{A}_1(1 - x - y - z) + \bar{A}_2 x + \bar{A}_3 y + \bar{A}_4 z \quad (13)$$

into $A_T^N(s)$ through the least-squares method (LSM); that is to say, we solve

$$\frac{\partial}{\partial \bar{A}_i} \int_0^1 dx \int_0^{1-x} dy \int_0^{1-x-y} dz$$
$$\times \left| A_T^N(s) - A_T^{LSM}(s) \right|^2 = 0. \quad (14)$$

(3) We apply the same procedure to ϵ_k, and obtain $\epsilon_T^{LSM}(s)$.

(4) We evaluate integral (2) replacing $A_T(s)$ and $\epsilon_T(s)$ with $A_T^{LSM}(s)$ and $\epsilon_T^{LSM}(s)$, respectively.

(5) We repeat the above steps for all tetrahedra.

Although the approximated matrix element $A_T^{LSM}(s)$ is discontinuous at boundaries of tetrahedra [see Fig. 2(b)], it is of no concern because we are interested only in the integrated value.

D. Implementation

We use a third-order polynomial $A_T^3(s)$ as $A_T^N(s)$ in our implementation. The sampling points used to construct $A_T^3(s)$ are the corners of the tetrahedron T (4 points) and the other 16 points given in Table I and Fig. 3. As a result, $A_T^3(s)$ becomes

$$A_T^3(s) = \frac{A_1}{2}u(u+1)(2-u) + \frac{A_2}{2}x(x+1)(2-x) + \frac{A_3}{2}y(y+1)(2-y) + \frac{A_4}{2}z(z+1)(2-z) - \frac{u^2 x}{6}(2A_5 + A_{14})$$

$$- \frac{x^2 y}{6}(2A_6 + A_{15}) - \frac{y^2 z}{6}(2A_7 + A_{16}) - \frac{z^2 u}{6}(2A_8 + A_{13}) - \frac{u^2 y}{6}(2A_9 + A_{11}) - \frac{x^2 z}{6}(2A_{10} + A_{12})$$

$$- \frac{y^2 u}{6}(2A_{11} + A_9) - \frac{z^2 x}{6}(2A_{12} + A_{10}) - \frac{u^2 z}{6}(2A_{13} + A_8) - \frac{x^2 u}{6}(2A_{14} + A_5) - \frac{y^2 x}{6}(2A_{15} + A_6) - \frac{z^2 y}{6}(2A_{16} + A_7)$$

$$+ (A_2 + A_4)xz(u+y) + (A_1 + A_3)uy(x+z) - \left(A_{17} + \frac{A_{10} + A_{12}}{2} + \frac{A_5 - A_{14}}{6} + \frac{A_{13} - A_8}{6} \right)xzu$$

$$- \left(A_{18} + \frac{A_9 + A_{11}}{2} + \frac{A_6 - A_{15}}{6} + \frac{A_{14} - A_5}{6} \right)xyu - \left(A_{19} + \frac{A_{10} + A_{12}}{2} + \frac{A_7 - A_{16}}{6} + \frac{A_{15} - A_6}{6} \right)xyz$$

$$- \left(A_{20} + \frac{A_9 + A_{11}}{2} + \frac{A_8 - A_{13}}{6} + \frac{A_{16} - A_7}{6} \right)yzu, \quad (15)$$

where $u = 1 - x - y - z$. By substituting it into (14), we obtain $A_T^{LSM}(s)$:

$$\bar{A}_i = \sum_{j=1}^{20} P_{ij} A_{k_j}, \quad (16)$$

where

$$\mathbf{P} = (\mathbf{P}^{(1)}, \mathbf{P}^{(2)}, \mathbf{P}^{(3)}, \mathbf{P}^{(4)}, \mathbf{P}^{(5)}), \quad (17)$$

$$\mathbf{P}^{(1)} = \frac{1}{1260} \begin{pmatrix} 1440 & 0 & 30 & 0 \\ 0 & 1440 & 0 & 30 \\ 30 & 0 & 1440 & 0 \\ 0 & 30 & 0 & 1440 \end{pmatrix}, \quad (18)$$

$$\mathbf{P}^{(2)} = \frac{1}{1260} \begin{pmatrix} -38 & 7 & 17 & -28 \\ -28 & -38 & 7 & 17 \\ 17 & -28 & -38 & 7 \\ 7 & 17 & -28 & -38 \end{pmatrix} = {}^t\mathbf{P}^{(4)}, \quad (19)$$

$$\mathbf{P}^{(3)} = \frac{1}{1260} \begin{pmatrix} -56 & 9 & -46 & 9 \\ 9 & -56 & 9 & -46 \\ -46 & 9 & -56 & 9 \\ 9 & -46 & 9 & -56 \end{pmatrix}, \quad (20)$$

$$\mathbf{P}^{(5)} = \frac{1}{1260} \begin{pmatrix} -18 & -18 & 12 & -18 \\ -18 & -18 & -18 & 12 \\ 12 & -18 & -18 & -18 \\ -18 & 12 & -18 & -18 \end{pmatrix}. \quad (21)$$
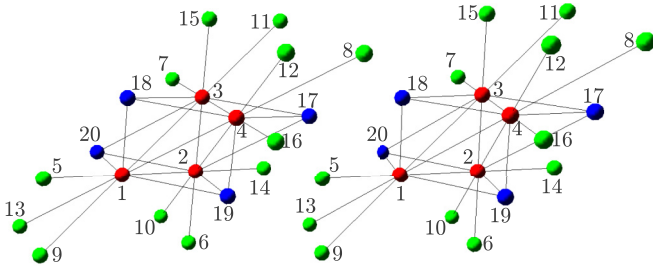
FIG. 3. (Color online) Points for constructing a third-order interpolation function (parallel stereogram). Red points denote the corners of T. The blue and green points are explained in Table I.

We go through the same procedure for the orbital energy $\epsilon_{\mathbf{k}}$.

We can consider this procedure in a different way: when we calculate the contribution from a tetrahedron, we use the linear tetrahedron method after we have replaced matrix elements and orbital energies with those given in (16). Using this idea, we represent the integration (1) as

$$\int d^3 k A_{\mathbf{k}} B(\epsilon_{\mathbf{k}}) = \sum_{\mathbf{k}} A_{\mathbf{k}} w_{\mathbf{k}}, \qquad (22)$$

where $w_{\mathbf{k}}$ is calculated as follows:

(1) We divide the BZ into tetrahedra.

(2) We calculate effective orbital energies as

$$\bar{\epsilon}_i = \sum_{j=1}^{20} P_{ij} \epsilon_{\mathbf{k}_j^T} \qquad (23)$$

for the corners of each tetrahedron.

(3) We calculate the effective weight $\bar{w}_i^T$ using the standard linear tetrahedron method with the effective orbital energy (23).

(4) $w_{\mathbf{k}}$ is calculated as

$$w_{\mathbf{k}} = \sum_{T} \sum_{i=1}^{4} \sum_{j=1}^{20} P_{ij} \bar{w}_i^T \delta\left(\mathbf{k} - \mathbf{k}_j^T\right). \qquad (24)$$

III. COMPARISON WITH OTHER INTEGRATION SCHEMES FOR ACTUAL CALCULATIONS

We implement our method in an *ab initio* electronic structure calculation code QUANTUM ESPRESSO [14] which uses plane waves to represent Kohn-Sham (KS) orbitals. Then, we test the effectiveness of the method through calculations of phonons in two systems, MgB_2 [15] and fcc lithium at a high pressure (20 GPa), based on DFPT [11] (Appendix A).

Magnesium diboride has the highest T_C (about 40 K) out of the known phonon-type superconductors. Many *ab initio* studies have been performed since it was discovered [12,16–19], revealing that the high T_C is a result of the strong interaction between intralayer vibrations of B atoms and their covalent bonding orbitals (σ bands) (Fig. 4). This strong coupling also softens phonon frequencies due to the screening of the ion-ion interaction; this screening occurs due to linear responses of σ electrons in the vicinity of the Fermi surfaces. We have to evaluate these responses accurately to determine the phonon frequencies precisely. Lithium exhibits a monatomic fcc structure at pressures between 7.5 and 39 GPa [20]. In this phase it becomes a superconductor. Its T_C increases with pressure up to 30 GPa [21–23] because of the growth of the electron-phonon interaction. The lower transverse acoustic mode at $\mathbf{q} \approx \overrightarrow{\Gamma K}$ couples with electrons most strongly in this material [13]. In this test, we consider the phonons of fcc Li at a pressure of 20 GPa.

We use norm-conserving pseudopotentials [24] in calculations of MgB_2; the cutoff energy of plane waves is set to 50 Ry. In the calculations of fcc lithium, we use an ultrasoft pseudopotential [25]. We treat the electrons in the $1s$ orbitals as valence electrons [26] and employ a cutoff energy of 80 Ry. In both of these applications, we use the GGA-PBE functional [27] and the first-order Hermite-Gaussian function [4,28] for broadening. We apply our method to the calculation of the frequency of the intralayer vibrational mode of B atoms at the A point in the BZ (Fig. 5, top left). The result of the improved tetrahedron method converges faster than that of the linear tetrahedron method; it converges with approximately 12^3 $\mathbf{k}$ points. If we use a broadening method with a small broadening width (0.01 Ry), the result converges at an unrealistically large number of $\mathbf{k}$ points (about 50^3 $\mathbf{k}$
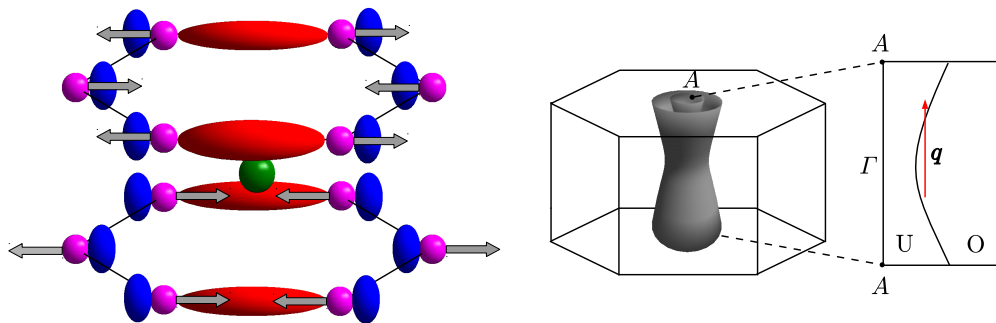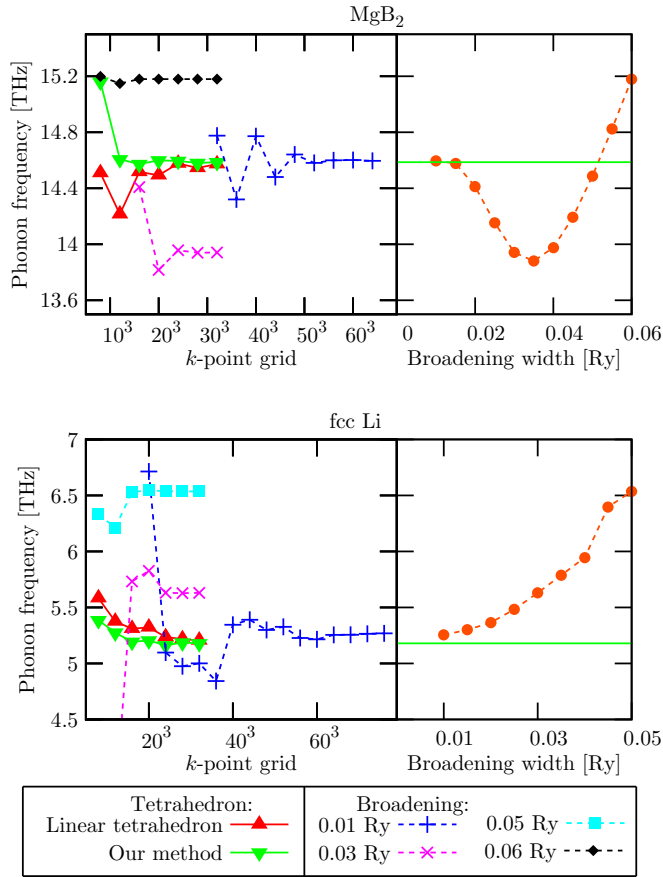

FIG. 4. (Color online) Left: The Mg-centered Wigner-Seits cell of MgB_2. Green and purple spheres indicate Mg and B atoms respectively. The σ orbital (blue and red isosurfaces of opposite signs) and the displacement pattern of the intralayer vibrational mode of the B atoms with wave number $\mathbf{q}$ at the A point (arrows) are also depicted. Right: Schematic illustration of the Fermi surfaces of the σ bands; the red arrow indicates the momentum vector of a phonon at the A point which connects occupied (O) and unoccupied (U) regions in the vicinity of the Fermi surface.

FIG. 5. (Color online) Left: k convergences of the frequencies of the intralayer vibrational mode of the B atoms at the A point in the BZ for MgB_2 (top) and the lower transverse acoustic mode at the K point in the BZ for fcc Li at 20 GPa (bottom) with a different k integration method. The upward-pointing and downward-pointing triangles with red and green solid lines are the results of the linear and improved tetrahedron methods; the plus signs, multiplication signs, squares, and diamonds with blue, purple, cyan, and black dashed lines denote the results of the broadening method for widths of 0.01, 0.03, 0.05, and 0.06 Ry, respectively. Lines are guides for the eyes. Right: The frequency of these modes converged about the number of k at each broadening width (circles with orange line); the green solid lines indicate the converged value obtained by our method.

points). On the other hand, using large broadening widths (0.03 Ry and 0.06 Ry), convergence occurs at a lower number of k points. However, results are far away from the one converged about the broadening width; the complicated dependence of the convergence on the broadening width is shown in the top-right panel of Fig. 5. The result cannot be represented by a simple function, so it is difficult to extrapolate to a broadening width of zero.

The bottom left panel of Fig. 5 shows the k convergence of the lower transverse acoustic mode at the K point in the BZ for fcc Li at 20 GPa calculated with the different integration schemes. Our method achieves convergence very quickly; it requires only 16^3 k points. In this system, the result of the broadening method is very sensitive to the broadening width; the error due to broadening is more than 25% at a width of

0.05 Ry; hence, the broadening method is not suitable for this calculation.

We will show how the accuracy of the phonon calculations affects the prediction of the superconducting transition temperature within the framework of the following McMillan formula [29,30]:

$$T_C = \frac{\omega_{\ln}}{1.2} \exp\left[\frac{-1.04(1+\lambda)}{\lambda - \mu^*(1 + 0.62\lambda)}\right]. \quad (25)$$

Here,

$$\lambda = \sum_{q\nu knn'} \frac{2}{D(\epsilon_F)\omega_{q\nu}}$$

$$\times \left|g^{q\nu}_{nkn'k+q}\right|^2 \delta(\epsilon_{nk} - \epsilon_F)\delta(\epsilon_{n'k+q} - \epsilon_F) \quad (26)$$

and

$$\ln(\omega_{\ln}) = \frac{1}{\lambda}\sum_{q\nu knn'} \frac{2}{D(\epsilon_F)\omega_{q\nu}} \ln(\omega_{q\nu})$$

$$\times \left|g^{q\nu}_{nkn'k+q}\right|^2 \delta(\epsilon_{nk} - \epsilon_F)\delta(\epsilon_{n'k+q} - \epsilon_F), \quad (27)$$

where $\omega_{q\nu}$ is the phonon frequency with the wave number q and the branch ν, ϵ_{nk} is the KS eigenvalue with the wave number k and the band index n, and $D(\epsilon_F)$ is the density of states per spin at the Fermi energy. The electron-phonon coupling constant $g^{q\nu}_{nkn'k+q}$ is written in the form

$$g^{q\nu}_{nkn'k+q} = \sum_{\tau\alpha} \frac{(\eta_{q\nu})_{\tau\alpha}}{\sqrt{M_\tau \omega_{q\nu}}} \left\langle n', k + q \left| \frac{\delta v_S}{\delta R_{\tau\alpha}(q)} \right| n, k \right\rangle, \quad (28)$$

where M_τ is a mass of an ion, $(\eta_{q\nu})_{\tau\alpha}$ is the unit displacement pattern of the phonon (q,ν), $|n,k\rangle$ is the KS orbital, and $\delta v_S/\delta R_{\tau\alpha}(q)$ is the linear response of the KS potential with respect to the distortion of the wave number q; τ and α are indices of an ion in the unit cell and a direction in the Cartesian coordinate, respectively. Although there are more precise methods to calculate T_C such as density functional theory for superconductors [31,32], we use this simple formula because we are only interested in changes in the results due to the k integration in the phonon calculations.

To evaluate the integrals in (26) and (27), we use the linear tetrahedron method with a q grid of $6 \times 6 \times 4$ ($8 \times 8 \times 8$) and a k grid of $24 \times 24 \times 18$ ($32 \times 32 \times 32$) for MgB_2 (fcc Li), respectively. Additionally, we calculate each $\omega_{q\nu}$ and $\delta v_S/\delta R_{\tau\alpha}(q)$ with different k grids and different k integration schemes.

Figure 6 shows the result of λ, $\omega_{\ln}$, and T_C from McMillan's formula ($\mu^* = 0.1$); in both the MgB_2 and Li cases, we obtain very fast k convergence using our method. Comparing the k converged result of our method to that of the broadening method with a width of 0.05 Ry, we can see a large overestimate of the phonon frequencies occurs when the broadening method is used, resulting in an underestimated λ and an overestimated $\omega_{\ln}$. Moreover, speeds of convergences about the broadening width for calculations of the λ and $\omega_{\ln}$ are very slow; these results have not reach the convergence even for the broadening width of 0.01 Ry; if we use smaller broadening width (such as 0.005 Ry), we need an unrealistic number of k points to obtain the k-converged result.
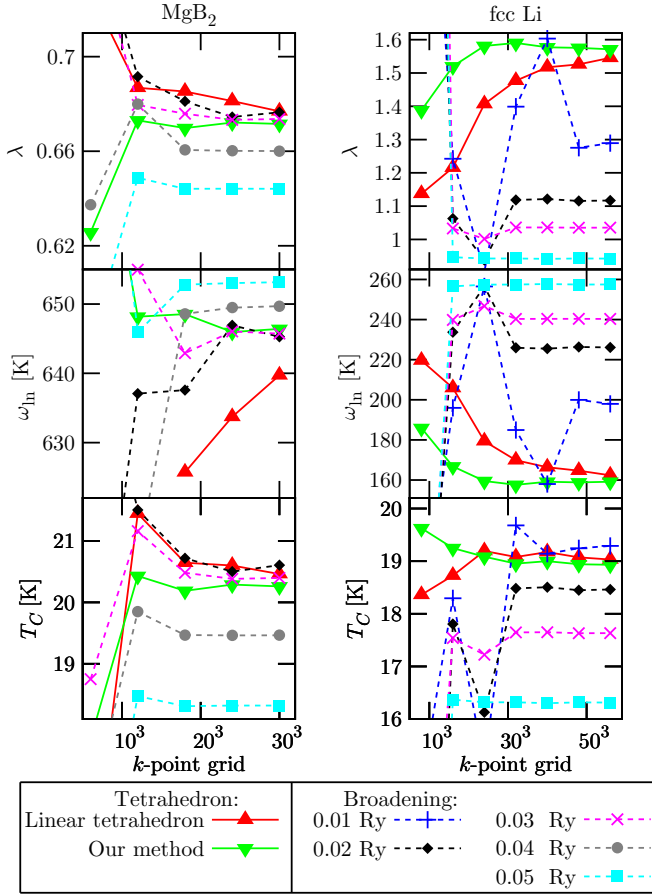
FIG. 6. (Color online) The $\boldsymbol{k}$ convergences of λ (top), $\omega_{\ln}$ (middle), and T_C from McMillan's formula (bottom) of MgB_2 (left) and fcc Li (right) calculated using $\omega_{q\nu}$ and $\delta v_S/\delta R_{\tau\alpha}(\boldsymbol{q})$ with different $\boldsymbol{k}$ integration schemes; the upward-pointing and downward-pointing triangles with red and green solid lines are the results of the linear and improved tetrahedron methods; the diamonds, plus signs, multiplication signs, squares, and circles with gray, blue, purple, black, and cyan dashed lines denote the results of broadening methods of widths 0.01, 0.02, 0.03, 0.04, and 0.05 Ry respectively. Lines are guides for the eyes.

IV. CONCLUSION

We introduced an improvement to the tetrahedron method based on the third-order interpolation and the least-squares method that reduces the number of $\boldsymbol{k}$ points required to obtain converged results of the BZ integrations. Our method is applicable to various kinds of $\boldsymbol{k}$ integration; in particular, it is efficient for calculations of phonons and response functions because the associated computational costs are large and the Blöchl correction is not applicable to these calculations. We demonstrated this effectiveness through calculations of phonon frequencies in MgB_2 and fcc Li.

APPENDIX A: CALCULATION OF WEIGHTS FOR DFPT

The integration weights for the DFPT calculations of phonon frequencies are different from those of the total energy, $\theta(\epsilon_F - \epsilon_{nk})$, or the density of states, $\delta(\epsilon - \epsilon_{nk})$. They are

$$W_{nn'k}^{(1)} = \frac{\theta(\epsilon_{n'k+q} - \epsilon_F)\theta(\epsilon_F - \epsilon_{nk})}{\epsilon_{nk} - \epsilon_{n'k+q}}, \qquad (A1)$$

$$W_{nn'k}^{(2)} = \theta(\epsilon_F - \epsilon_{nk})\theta(\epsilon_{nk} - \epsilon_{n'k+q}). \qquad (A2)$$

In integrations with weights that contain products of two step functions, only regions where both Heaviside functions become 1 contribute to the results; therefore, we divide the tetrahedra two times to cut out these regions (Fig. 7). We will explain how to calculate $W_{nn'k}^{(1)}$.

(1) We divide a subcell into six tetrahedra.

(2) We cut out one or three tetrahedra T' where $\theta(\epsilon_F - \epsilon_{nk}) = 1$ from tetrahedron T and evaluate $\epsilon_{nk}, \epsilon_{n'k+q}$ at the corners of T'' as

$$\epsilon_{T'i} = \sum_{j=1}^{4} F_{ij}(\epsilon_F - \epsilon_{T1}, \ldots, \epsilon_F - \epsilon_{T4})\epsilon_{Tj}, \qquad (A3)$$

through linear interpolation (Appendix B). Here $\epsilon_{T1}, \ldots, \epsilon_{T4}$ and $\epsilon'_{T1}, \ldots, \epsilon'_{T4}$ are ϵ_{nk} and $\epsilon_{n'k+q}$, respectively, on the corners of T, where $\epsilon_{T1} \leqslant \epsilon_{T2} \leqslant \epsilon_{T3} \leqslant \epsilon_{T4}$.

(3) We cut out one or three tetrahedra T'' where $\theta(\epsilon_{n'k+q} - \epsilon_F) = 1$ from tetrahedron T'. The orbital energies are calculated as

$$\epsilon_{T''i} = \sum_{j=1}^{4} F_{ij}(\epsilon'_{T'1} - \epsilon_F, \ldots, \epsilon'_{T'4} - \epsilon_F)\epsilon_{T'j}. \qquad (A4)$$

(4) The weights of the corners of T'' are (Appendix C)

$$W_{T''i}^{(1)} = -V_{T''} \sum_{j=1, j\neq i}^{4} \frac{d_j^2\left(\frac{\ln d_j - \ln d_i}{d_j - d_i}d_j - 1\right)}{\prod_{k=1, k\neq j}^{4}(d_j - d_k)}, \qquad (A5)$$
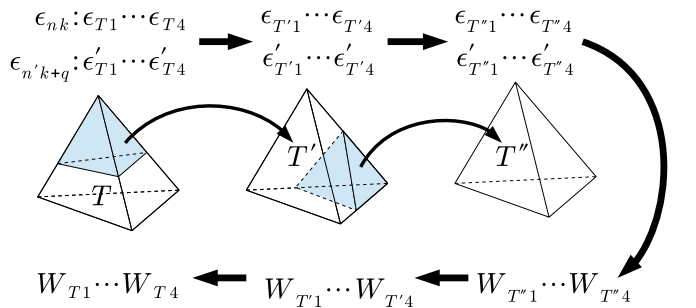
where $d_i = \epsilon'_{T''i} - \epsilon_{T''i}$.

FIG. 7. (Color online) Flow of the calculation of weights. We divide the tetrahedra two times to cut out regions where two Heaviside functions become one.
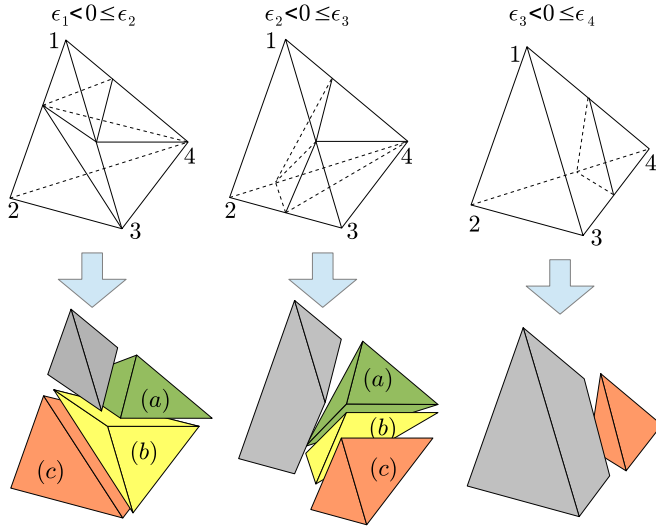
FIG. 8. (Color online) How to divide a tetrahedron in the case of $\epsilon_1 \leqslant 0 < \epsilon_2$ (left), $\epsilon_2 \leqslant 0 < \epsilon_3$ (center), and $\epsilon_3 \leqslant 0 < \epsilon_4$ (right).

(5) We calculate the weights of the corners of T' from those of T'':

$$W_{T'i}^{(1)} = \sum_{j=1}^{4} F_{ji}(\epsilon_{T'1}' - \epsilon_{\mathrm{F}}, \ldots, \epsilon_{T'4}' - \epsilon_{\mathrm{F}}) W_{T''j}^{(1)}. \quad \text{(A6)}$$

(6) We calculate the weights of the corners of T from those of T':

$$W_{Ti}^{(1)} = \sum_{j=1}^{4} F_{ji}(\epsilon_{\mathrm{F}} - \epsilon_{T1}, \ldots, \epsilon_{\mathrm{F}} - \epsilon_{T4}) W_{T'j}^{(1)}. \quad \text{(A7)}$$

(7) Finally, we sum up the contributions from all tetrahedra:

$$W_{nn'k}^{(1)} = \sum_{T=1}^{6N_k} \sum_{i=1}^{4} W_{Ti}. \quad \text{(A8)}$$

APPENDIX B: HOW TO DIVIDE A TETRAHEDRON

We will explain how to cut out tetrahedra T' in the case of $\theta(\epsilon) = 1$ from tetrahedron T. We represent ϵ_{nk} at the corners of T as $\epsilon_1, \ldots, \epsilon_4$, where $\epsilon_1 \leqslant \epsilon_2 \leqslant \epsilon_3 \leqslant \epsilon_4$. We define $a_{ij} = -\epsilon_j/(\epsilon_i - \epsilon_j)$. In all cases

$$V_{T'} = V_T |\det(F)|. \quad \text{(B1)}$$

(1) $0 \leqslant \epsilon_1$. We cut out no tetrahedra because $\theta(\epsilon)$ becomes 1 over the entire tetrahedron in this case:

$$F = \begin{pmatrix} 1 & 0 & 0 & 0 \\ 0 & 1 & 0 & 0 \\ 0 & 0 & 1 & 0 \\ 0 & 0 & 0 & 1 \end{pmatrix}. \quad \text{(B2)}$$

(2) $\epsilon_1 \leqslant 0 < \epsilon_2$. Three tetrahedra are cut out (Fig. 8, left):

$$(a) \qquad F = \begin{pmatrix} a_{12} & a_{21} & 0 & 0 \\ a_{13} & 0 & a_{31} & 0 \\ a_{14} & 0 & 0 & a_{41} \\ 0 & 0 & 0 & 1 \end{pmatrix}, \quad \text{(B3)}$$

$$(b) \qquad F = \begin{pmatrix} a_{12} & a_{21} & 0 & 0 \\ a_{13} & 0 & a_{31} & 0 \\ 0 & 0 & 1 & 0 \\ 0 & 0 & 0 & 1 \end{pmatrix}, \quad \text{(B4)}$$

$$(c) \qquad F = \begin{pmatrix} a_{12} & a_{21} & 0 & 0 \\ 0 & 1 & 0 & 0 \\ 0 & 0 & 1 & 0 \\ 0 & 0 & 0 & 1 \end{pmatrix}. \quad \text{(B5)}$$

(3) $\epsilon_2 \leqslant 0 < \epsilon_3$. Three tetrahedra are cut out (Fig. 8, center):

$$(a) \qquad F = \begin{pmatrix} a_{13} & 0 & a_{31} & 0 \\ a_{14} & 0 & 0 & a_{41} \\ 0 & a_{24} & 0 & a_{42} \\ 0 & 0 & 0 & 1 \end{pmatrix}, \quad \text{(B6)}$$

$$(b) \qquad F = \begin{pmatrix} a_{13} & 0 & a_{31} & 0 \\ 0 & a_{23} & a_{32} & 0 \\ 0 & a_{24} & 0 & a_{42} \\ 0 & 0 & 0 & 1 \end{pmatrix}, \quad \text{(B7)}$$

$$(c) \qquad F = \begin{pmatrix} a_{13} & 0 & a_{31} & 0 \\ 0 & a_{23} & a_{32} & 0 \\ 0 & 0 & 1 & 0 \\ 0 & 0 & 0 & 1 \end{pmatrix}. \quad \text{(B8)}$$

(4) $\epsilon_3 \leqslant 0 < \epsilon_4$. One tetrahedron is cut out (Fig. 8, right):

$$F = \begin{pmatrix} a_{14} & 0 & 0 & a_{41} \\ 0 & a_{24} & 0 & a_{42} \\ 0 & 0 & a_{34} & a_{43} \\ 0 & 0 & 0 & 1 \end{pmatrix}. \quad \text{(B9)}$$

APPENDIX C: CALCULATION OF $W_{T''}^{(1)}$

We represent the matrix elements at the corners of the tetrahedron as $f_1, \ldots, f_4$. We evaluate the integral

$$\left\langle \frac{A}{d} \right\rangle_{T''} = \int_{T''} d^3k \frac{A_k}{d_k} \quad \text{(C1)}$$

using linear interpolation to obtain

$$A_{T''} \approx 6V'' \int_0^1 dx \int_0^{1-x} dy \int_0^{1-x-y} dz$$
$$\times \frac{A_1 + (A_2 - A_1)x + (A_3 - A_1)y + (A_4 - A_1)z}{d_1 + (d_2 - d_1)x + (d_3 - d_1)y + (d_4 - d_1)z}$$
$$\equiv \sum_{i=1}^{4} A_i W_{T''i}, \quad \text{(C2)}$$

where

$$W_{T''i} = 6V'' \int_0^1 dx_1 \int_0^1 dx_2 \int_0^1 dx_3 \int_0^1 dx_4$$
$$\times \frac{x_i \delta(x_1 + x_2 + x_3 + x_4 - 1)}{d_1 x_1 + d_2 x_2 + d_3 x_3 + d_4 x_4}. \quad \text{(C3)}$$

This in turn yields (A5).

[1] P. Hohenberg and W. Kohn, Phys. Rev. **136**, B864 (1964).

[2] J. Perdew, M. Emzerhof, and K. Burke, J. Chem. Phys. **105**, 9982 (1996).

[3] L. Hedin, Phys. Rev. **139**, A796 (1965).

[4] M. Methfessel and A. T. Paxton, Phys. Rev. B **40**, 3616 (1989).

[5] O. Jepsen and O. K. Andersen, Solid State Commun. **9**, 1763 (1971).

[6] J. Rath and A. J. Freeman, Phys. Rev. B **11**, 2109 (1975)

[7] S. Y. Savrasov, Phys. Rev. Lett. **69**, 2819 (1992).

[8] S. Y. Savrasov and D. Y. Savrasov, Phys. Rev. B **54**, 16487 (1996).

[9] T. Fujiwara, S. Yamamoto, and Y. Ishii, J. Phys. Soc. Jpn. **72**, 777 (2003).

[10] P. E. Blöchl, O. Jepsen, and O. K. Andersen, Phys. Rev. B **49**, 16223 (1994).

[11] S. Baroni, S. de Gironcoli, A. Dal Corso, and P. Giannozzi, Rev. Mod. Phys. **73**, 515 (2001).

[12] M. Calandra, G. Profeta, and F. Mauri, Phys. Rev. B **82**, 165111 (2010).

[13] T. Bazhirov, J. Noffsinger, and M. L. Cohen, Phys. Rev. B **82**, 184509 (2010).

[14] P. Giannozzi *et al*., J. Phys.: Condens. Matter **21**, 395502 (2009); http://www.quantum-espresso.org/.

[15] J. Nagamatsu, N. Nakagawa, T. Muranaka, Y. Zenitani, and J. Akimitsu, Nature (London) **410**, 63 (2001).

[16] Y. Kong, O. V. Dolgov, O. Jepsen, and O. K. Andersen, Phys. Rev. B **64**, 020501 (2001).

[17] K.-P. Bohnen, R. Heid, and B. Renker, Phys. Rev. Lett. **86**, 5771 (2001).

[18] H. J. Choi, D. Roundy, H. Sun, M. L. Cohen, and S. G. Louie, Phys. Rev. B **66**, 020513 (2002).

[19] A. Eiguren and C. Ambrosch-Draxl, Phys. Rev. B **78**, 045124 (2008).

[20] M. Hanfland, K. Syassen, N. Christensen, and D. Novikov, Nature (London) **408**, 174 (2000).

[21] S. Deemyad and J. S. Schilling, Phys. Rev. Lett. **91**, 167001 (2003).

[22] V. Struzhkin, M. Eremets, W. Gan, H. Mao, and R. Hemley, Science **298**, 1213 (2002).

[23] K. Shimizu, H. Ishikawa, D. Takao, T. Yagi, and K. Amaya, Nature (London) **419**, 597 (2002).

[24] D. R. Hamann, M. Schlüter, and C. Chiang, Phys. Rev. Lett. **43**, 1494 (1979).

[25] D. Vanderbilt, Phys. Rev. B **41**, 7892 (1990).

[26] We used the pseudopotential Li.pbe-s-rrkjus_psl.0.2.1.UPF from http://www.quantum-espresso.org.

[27] J. P. Perdew, K. Burke, and M. Ernzerhof, Phys. Rev. Lett. **78**, 1396 (1997).

[28] S. de Gironcoli, Phys. Rev. B **51**, 6773 (1995).

[29] W. L. McMillan, Phys. Rev. **167**, 331 (1968).

[30] R. Dynes, Solid State Commun. **10**, 615 (1972).

[31] L. N. Oliveira, E. K. U. Gross, and W. Kohn, Phys. Rev. Lett. **60**, 2430 (1988).

[32] M. Lüders, M. A. L. Marques, N. N. Lathiotakis, A. Floris, G. Profeta, L. Fast, A. Continenza, S. Massidda, and E. K. U. Gross, Phys. Rev. B **72**, 024545 (2005).